Numerical Investigation of the Hydrodynamics of Split-and-Recombination and Multilamination Microreactors

Lionel S. Méndez-Portillo, Mourad Heniche, Charles Dubois, and Philippe A. Tanguy
Dept. of Chemical Engineering, École Polytechnique de Montréal, P.O. Box 6079, Station Centre-Ville, Montreal, QC, Canada H3C 3A7

DOI 10.1002/aic.13858
Published online June 25, 2012 in Wiley Online Library (wileyonlinelibrary.com).

The hydrodynamics and residence time distribution (RTD) of two microreactors based on the split-and-recombination (SAR), and multilamination mixing mechanisms, respectively were investigated. It was found that the design of the distribution manifolds of the SAR mechanism produces an unbalanced flow distribution. For feeding ratios different than one, bypassing and recirculation occur within the SAR manifolds. For equal flow rates the SAR flow behavior can be accurately described by the pure convection model. The manifold used in the multilamination microreactor achieves a homogeneous distribution of flow and its interdigital mixing structure generates an alternated pattern of fluid layers which is maintained for Re *140. After this point the ordered arrangement is broken and two large segregated zones are formed. In the absence of molecular diffusion both microreactors reach limiting values of scale and intensity of segregation that were found to be independent of the energy applied to the system.* © 2012 American Institute of Chemical Engineers *AIChE J,* 59: 988–1001, 2013

Keywords: micromixer, microreactor, multilamination, split-and-recombination, RTD

Introduction

In the rapidly developing field of chemical microprocess engineering, microreaction technology is seen as a powerful approach for process intensification. Many applications can be thought of in the chemical industry, and polymer reaction engineering is certainly one field that could exploit the theoretical benefits of microreaction technology. Indeed, polymerization reactions are usually exothermic and highly sensitive to the level of mixing of the reactants and can benefit from the high heat-transfer rates and efficient mixing allowed in microreactors. Whereas a low throughput can be anticipated from microreactors due to their characteristic small active volume, high selectivity and yield[1–3] can favorably impact the overall performance of a polymerization process in the microscale. This compromise between low throughput and reaction performance makes microreaction technology an attractive alternative for targeted applications such as on-demand production of polymers or fine chemicals. Selectivity and overall yield of a reaction are related to the degree of mixing and the time spent by the reactants inside the chemical reactor which in turn are governed by diffusion effects and the specific flow patterns of the reaction vessel. Thus, knowledge of the spatial and temporal mixing characteristics of the flow system is necessary to predict yield and conversion of chemical reactions.

The flow patterns inside a chemical reactor have a direct impact on the amount of time and contacting area of the reactants, which can lead to unexpected concentration gradients and unreacted material. The distinctive flow patterns of any chemical reactor are the result of the relationship between the fluid properties, flow conditions, and the geometry of the vessel. Proper knowledge of these contacting flow patterns is required to predict the behavior of a continuous flow reactor. Thus, direct visualization of flow patterns is one of the most appropriate approaches to understand three-dimensional (3-D) flow phenomena in chemical reactors. However, direct visualization is not possible in microreactors that are constructed from nontransparent materials. Microfluidic devices are usually composed by several microchannels in parallel and in some cases by different flow sections in serial arrangements. This generates intricate flow paths that lead to difficult interpretation of experimental results. Furthermore, the performance of the distribution manifolds embedded in microreactors plays a critical role on the homogeneous distribution of the flow, and, consequently, on the level of concentration of reactants in a parallel microchannel network. Inhomogeneous flow distribution may lead to poor reaction selectivity and degrade the overall yield of the process.

A series of investigations used CFD simulations to gain a better insight of the flow patterns of new micromixing mechanisms;[4–7] on the optimization of microchannel shapes and distribution manifolds;[8–12] on the characterization of mixing efficiency of microdevices;[13–22] and on the calculation of numerically based residence time distributions (RTD).[23–27] Most of the aforementioned studies focused on T-junctions and the staggered-herringbone mixer (SHM). Presently, there is a large family of available microreactor models and knowledge about their hydrodynamic performance is a key requirement to find suitable applications.

Correspondence concerning this article should be addressed to C. Dubois at charles.dubois@polymtl.ca.

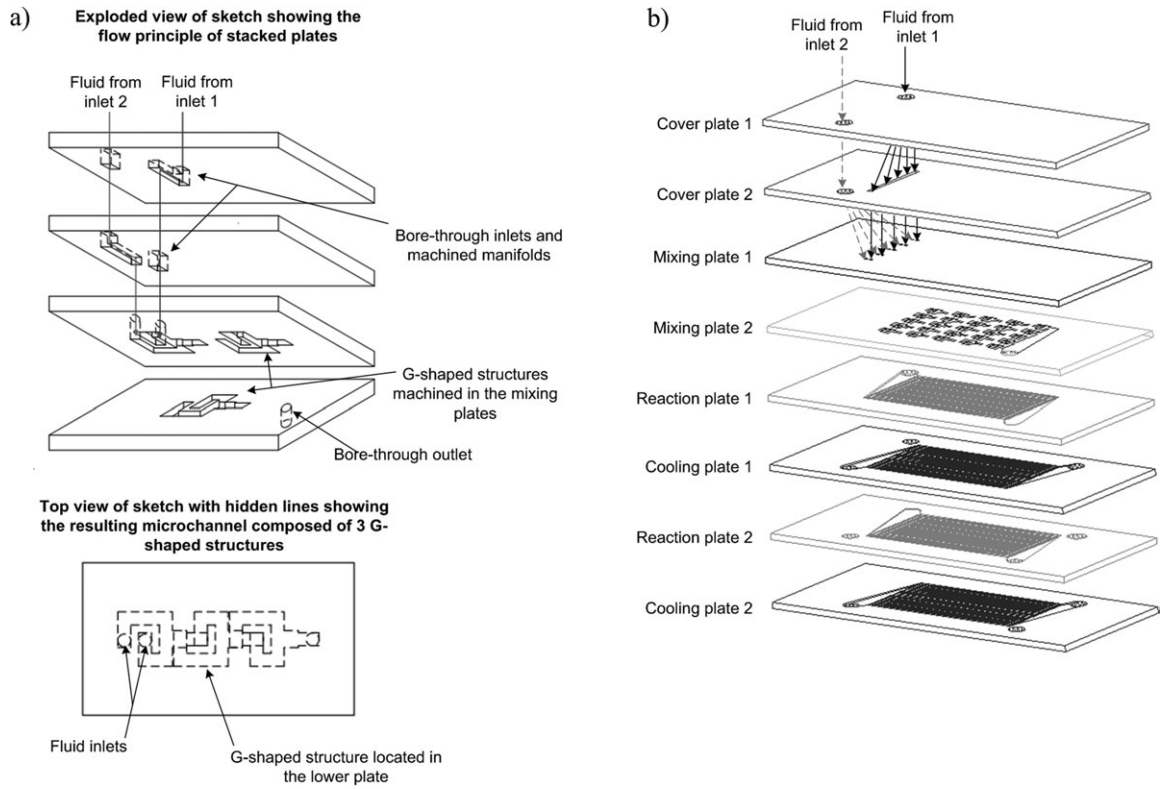

Figure 1. Schematic of the SAR microreactor plates (a) stacking order, and (b) flow principle.

We have previously conducted an experimental characterization[28] of the performance of two microreactors known as potential candidates for industrial applications. One unit was a prototype design using the split-and-recombination (SAR) mixing principle, while the other was an already commercialized model using the mixing mechanism of multilamination of flow by means of an interdigital structure. The results indicated the possibility of bypassing and/or recirculation. Since visual inspection is restricted in the microreactors investigated, numerical flow simulations (CFD) can be used as a useful complementary tool for the analysis of the fluid mechanics inside these microfluidic devices.

In the forthcoming, our objective is to provide further insight on the hydrodynamic performance and RTD of the two microreactors by means of CFD, and especially to clarify the extent of the role of the manifold design on the flow distribution in the microchannel network.

Description of Micrometors

Two microreactors have been considered in this work. A prototype microreactor featuring a split-and-recombination mechanism (further referenced as SAR) was provided by Atotech GmbH (Berlin, Germany). The SAR microreactor consists of a stacked arrangement of 8 plates (Figure 1)

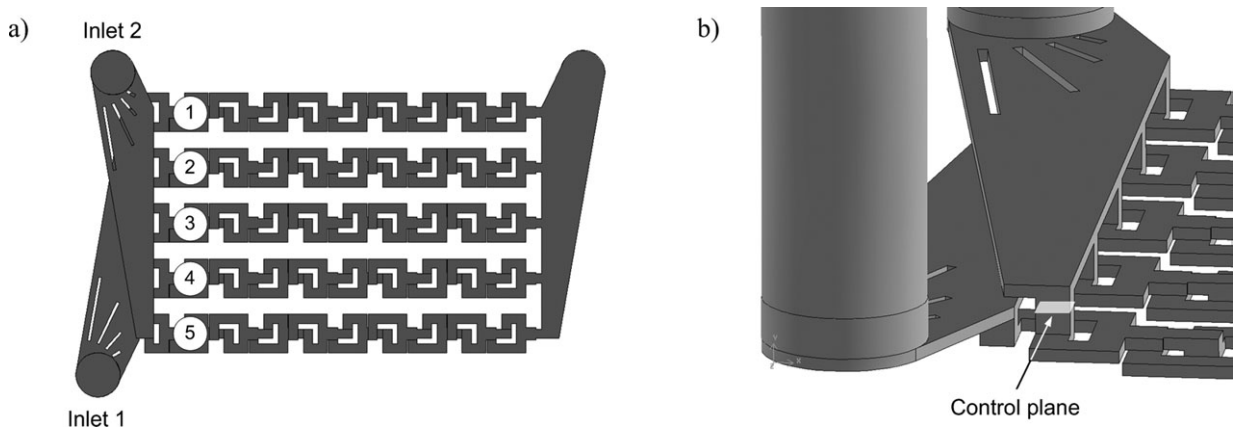

Figure 2. Flow path of the mixing section of the SAR microreactor (a) top view of the complete mixing section, and (b) isometric detail of each manifold attaching to the five G-shaped structures.

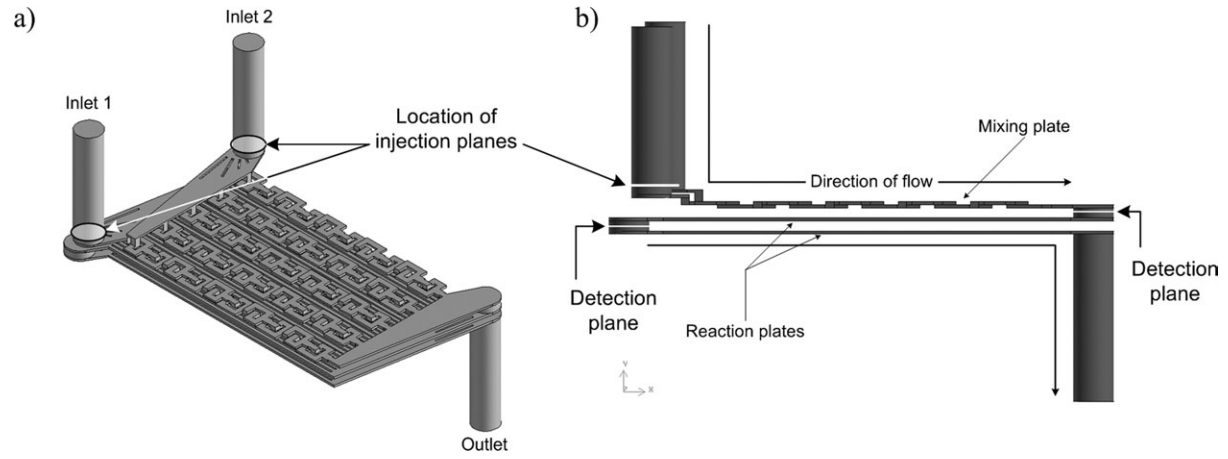

Figure 3. Isometric (a) and lateral (b) views of the 3-D flow path of the complete mixing and reaction sections featured by the SAR microreactor including inlet and outlet ports.

where the mixing section is created by two plates featuring a G-shaped structure[29–31] employed to arrange the splitting elements longitudinally along the flow direction. The resulting microchannel network consists of five long mixing channels composed of 10 G-shaped structures (Figure 2).

The solid model of the resulting flow path of the SAR microreactor used for the simulations is presented in Figure 3. The distribution and collection manifolds are manufactured with a trapezoidal shape. This type of manifold has been applied in other parallel channel microdevices[30,31] and proposed as the optimized shape that minimizes space time under the constraint of flow uniformity.[11,12]

The second microreactor is a liquid/liquid microreactor (LLMR) acquired from IMM GmbH (Mainz, Germany) under the model designation LLMR-MIX-SI, and is based on the multilamination of flow by means of an interdigital structure. The LLMR microreactor[2,32] consists of a stack of four machined plates. The first plate is composed of two inlets that feed the reactants into a mixer inlay in which the fluids are contacted in a bilayer configuration. The multilamination mechanism takes place in the mixer inlay (Figure 4). The solid model of flow path of the LLMR is presented in Figure 5. For the purpose of schematic representation, the reaction channels of the LLMR in Figure 5 have been shortened to 10 mm. However, during the numerical simulations the original microchannel length of 75 mm was used.

The geometric characteristics of the microchannels considered in this investigation are given in Table 1. Further details of their assembly and flow characteristics can be found elsewhere.[28] The computer-aided design solid models of the 3-D flow path of the microreactors were based on the blueprints provided by the manufacturer in the case of the SAR, and on geometrical values and sketches disclosed in the user assembly manual in the case of the LLMR. The volumes of the 3-D models are accurate to $\pm 1\%$ of the values obtained experimentally except for the mixing section of the SAR which is almost three times higher.

Numerical Methodology

The characterization of mixing efficiency in microdevices[13–22] is usually based on the analysis of striation thickness and striation rates, the Lyapunov exponent, and statistical parameters such as the coefficient of variance. A more robust or unified analysis such as the spectral theory proposed by Cerbelli[33] could also be used. In that work, Cerbelli discussed the limitations of applying fundamental parameters such as the Lyapunov exponent when evaluating practical applications. Thus, a two-step numerical approach previously referenced as the decoupled CFD-mixing approach[34] is followed in this investigation. Such strategy has been applied for the numerical characterization of macroscopic static mixers[34–36] and microfluidic devices.[13,16,25–27] The first step consists of the computation of the flow variables (e.g., velocity and pressure) in the flow vessel geometry by means of CFD. The second step consists of analyzing the mixing performance and the residence time distribution (RTD) by means of the particle tracking technique. One limitation of this approach is that the effect of the viscosity ratio between the fluids to be mixed is not taken into account. However, its application is useful for certain mixing systems where the fluids exhibit similar viscosities upon contact, e.g., monomers and organic solvents in continuous free-radical polymerization processes.

Scale and intensity of segregation

In the context of CFD the mixing performance is usually evaluated by the concepts of scale and intensity of segregation proposed by Danckwerts[37] to describe the mixing process of two miscible liquid species. The scale of segregation is a measure of the size of the clumps that result from a

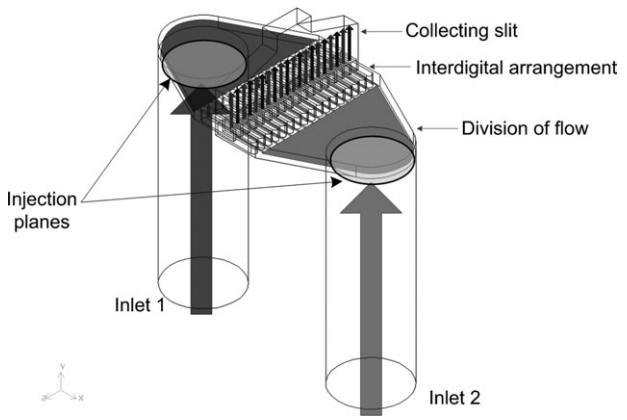

Figure 4. Schematic of the interdigital inlay of the LLMR in which multilamination takes place.

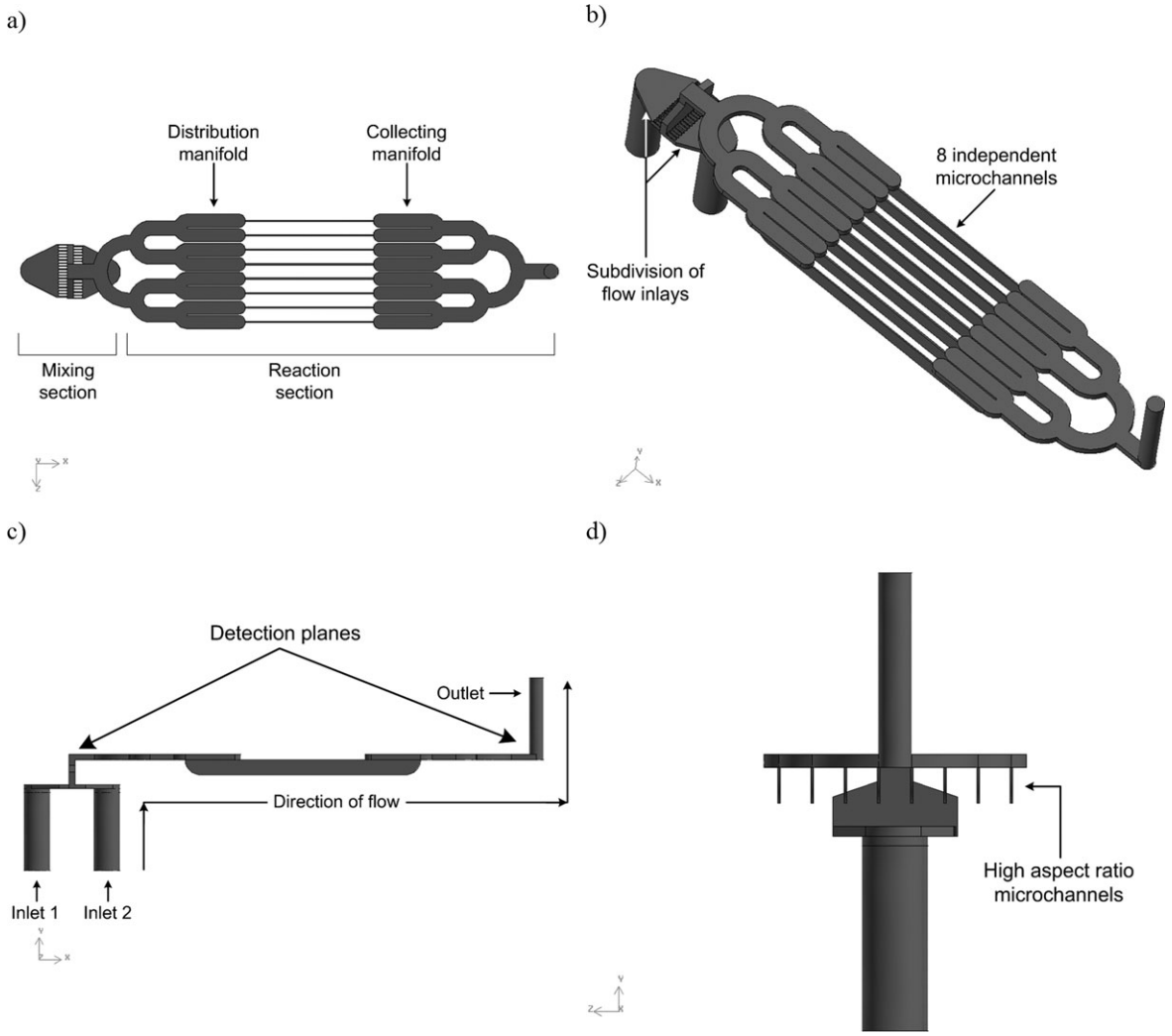

Figure 5. Views of the LLMR flow path with inlets and outlet ports (a) top, (b) isometric, (c) front, and (d) lateral.

breakup mechanism undergone by the two-fluid species. The intensity of segregation is a measure of the homogeneity of the two fluids across the boundaries of said clumps. Therefore, the scale and intensity of segregation are, respectively, related to the dispersive and distributive characteristics of the system.

In a mixture composed of species A and B, the scale of segregation is estimated by measuring the total concentration of one component in the mixture along a straight line joining two points in the reference plane of interest. The content J of species A in a line-sample of length X is defined by

$$J = \int_0^X a \, dx \tag{1}$$

where a is the concentration of A at a point distance x from one end of the line. If content J is determined for a large number of such line-samples in different regions of the mixture then the scale of segregation can be determined as

$$S_s = \frac{\sigma_J^2}{2X\sigma_a^2} \tag{2}$$

where σ^2 represents, respectively, the variances of J and a which are defined by

$$\sigma_J^2 = \overline{(J - \bar{a}X)^2} \tag{3}$$

$$\sigma_a^2 = \overline{(a - \bar{a})^2} \tag{4}$$

The intensity of segregation is a statistical parameter defined by Danckwerts[37] as

Table 1. Geometrical Values of the Microchannels used for Simulations

Microreactor	Section	Number of channels	Width (mm)	Height (mm)	Length (mm)	Volume experimental (μL)	Volume 3D model (μL)
SAR	Mixing	5	0.5	0.15	48.1	20	57.2
	Reaction	31	0.3	0.15	23.6	107	106.7
LLMR	Mixing	36	0.045	0.25	0.9	4	3.8
	Reaction	8	0.07	0.9	75	132	132.1

$$I_s = \frac{\sigma_a^2}{\bar{a} \cdot \bar{b}} \equiv \frac{\sigma_b^2}{\bar{a} \cdot \bar{b}} \tag{5}$$

where σ^2 represents the variance, a and b represent the concentrations of two different miscible species in terms of their volume fractions. The intensity of segregation I_s characterizes the extent to which the concentration of any of the two species in a delimited clump departs from the mean value of the mixture. As defined in Eq. 5, the intensity of segregation has a value of 0 when the concentration is uniform throughout all the clumps, and a value of 1 in a complete segregated state when the concentration in any clump is either only a or b.

Danckwerts[37] states that during the mixing of two miscible liquids the value of I_s is progressively reduced by the effect of molecular diffusion and not directly affected by the mechanical process of mixing. Thus, in the absence of diffusion the mixture would remain "grainy" or segregated. Relying on the statistical nature of the definition of intensity of segregation the particle tracking method has been exploited for the mixing characterization of microfluidic devices,[13,16,25] and at least one example of a stochastic approach (e.g., random walk model) has been coupled with this method to account for the effect of molecular diffusion.[26,27]

In this investigation we translate the concepts proposed by Danckwerts[37] to estimate the scale (S_s), and intensity (I_s), of segregation by means of the particle tracking method. The calculation of S_s and I_s is based on the spatial distribution of the tracer particles *positions* detected at specific reference planes perpendicular to the flow direction. The concentration of the particles positions is quantified as a function of predefined spatial regions or grid cells. The cell size, which can be viewed as the clump size in the Danckwerts definition, will dictate the level of resolution for the estimation of I_s. This level of resolution has been previously addressed,[38,39] and ideally there should be a grid cell for each particle injected. Thus, during the postprocessing stage of our methodology, we defined the grid size accordingly to the number of tracer particles arrived at the reference plane. The intensity of segregation estimated by the particle tracking method is the result of mechanistic effects only and disregards the effect of molecular diffusion. However, these mechanistic effects are of great importance in laminar flow systems that promote intensive radial mixing by means of split-and-recombination mechanisms, e.g., static mixers, microreactors. Due to the nature of the geometries analyzed in this investigation the scale and intensity of segregation are evaluated as a function of the flow conditions at a constant downstream position located at the outlet plane of the mixing sections of the microreactors.

The coefficient of variation *COV* is a statistical parameter frequently used to quantify the degree of mixing in continuous flow systems by means of CFD.[13,34–36] Statistically the *COV* is defined as the ratio of the standard deviation of a variant divided by the mean value of its distribution

$$COV_a = \frac{s_a}{\bar{a}} \tag{6a}$$

where s_a is the standard deviation of the concentration of species a defined as

$$s_a = \sqrt{\frac{1}{N-1} \cdot \sum_{i=1}^{N} (a_i - \bar{a})^2} \tag{6b}$$

It is usually stated that the *COV* varies from 0 to 1 with zero indicating a complete mixed stated while 1 represents complete segregation. The *COV* is a measure of relative variability about the mean and is recommended that this coefficient be used in ratio form and not as a percentage since it can readily exceed unity.[40] Values of $COV > 1$ are statistically possible even if volume fractions are used when a certain number of grid cells exhibit a concentration that is far greater than the mean. Thus, the use of *COV* to characterize the degree of segregation between 0 and 1 from Eq. 6 should be taken with care. In this study, the concept of intensity of segregation was chosen since the values of I_s as defined in Eq. 5 consistently vary between 0 and 1.

Residence time distribution

Two approaches can be followed for the numerical calculation of residence time distributions (RTD) in continuous flow systems, where distribution functions at a given cross section can be reproduced from (1) the concentration of species obtained by solving the continuity and convection-diffusion equations, and (2) the residence time of massless particles injected in the flow field.

Nauman[41] has raised concerns about the capabilities of CFD codes to account for the low-fluid velocities near the walls of the system, which can pose practical problems during the calculation of numerically based RTD. A strategy of particle restitution has been applied to macroscopic static mixers[42] and recently to microfluidic devices[25] to conserve the tracer particles that are lost in the region near the walls. In turn, this strategy has been questioned[43] since the reinstated particles do not conserve their flow history, and, thus, the theoretical criteria of infinite mean in the absence of molecular diffusion is not met.

However, according to Nauman[44] the exit-age distribution function in laminar flow systems without diffusion asymptotically approaches a dependence of t^{-3}, therefore, producing a finite mean. It has been demonstrated[45] that such a distribution has an infinite first moment with an asymptote proportional to t^{-2} when the RTD is weighted by surface area and not by volumetric flow rate. Nauman[45] states that in a laminar flow system, the exit-age distribution function weighted by volumetric flow rate will exhibit a first moment equal to V/Q even in the absence of molecular diffusion, with V being the total volume of the flow vessel, and Q the total volumetric flow rate.

The weighting of the tracked particles by volumetric flow rate is performed by assigning to each particle a fraction of the volumetric flow rate $\Delta Q_i = v_n \cdot \Delta A$, where v_n is the velocity normal to the inlet surface evaluated at the inlet surface, and ΔA is the area of the inlet associated with each particle. Each volume fraction is calculated relatively to the radial position $r_i(x,y)$ of each particle over the area A_{in} of the inlet tube as

$$\Delta Q_i = 2v\left(1 - \left(\frac{r_i}{R}\right)^2\right)\left(\frac{A_{in}}{N_t}\right) \tag{7}$$

where v is the mean flow velocity, R is the radius of the inlet tube, and N_t is the total number of tracer particles. The exit-age distribution function is then obtained by constructing a histogram of the volume fractions and their corresponding residence times. The ratio $\Delta Q_i/Q$ represents the fraction of particles having a residence time equal to t_i. Due to the

Table 2. Flow Conditions considered in the Simulations

Condition	Q (mL/min) Inlet 1	Inlet 2	Total	Flow ratio (r_Q)
1	0.1	0.1	0.2	1
2	0.1	1.0	1.1	0.1
3	0.1	10.0	10.1	0.01
4	0.5	0.5	1.0	1
5	1.0	1.0	2.0	1
6	10.0	10.0	20.0	1

discrete nature of the results the bin size at each frequency count must be defined prior to the construction of the histogram. The shape of the histogram is largely dependent on the choice of the bin size. If a large bin size is chosen the spike rate of the distribution cannot be accurately represented. On the contrary, if the bin size is too small the time histogram fluctuates greatly, and the underlying rate cannot be discerned. During the RTD analysis of flow vessels the shape of the histogram, that is, the RTD curve, is of critical importance for diagnosing purposes of special flows such as bypassing, recirculation or stagnancy. Thus, the relevance of selecting an appropriate bin size for such applications is evident.

Several methods exist to define the bin size of a histogram depending on the number of available data points. One robust criterion frequently used in statistical analysis is the Freedman-Diaconis estimator,[46] which relies on the calculation of the first and third interquartiles, and, thus, is not as susceptible to fluctuations as other estimators relying simply on the variance. More recently, a histogram bin width optimization method was developed by Shimazaki and Shinomoto[47] which is based on the minimization of the mean integrated squared error (MISE) of a preliminary histogram fitted to the underlying rate of the available data. In this method, an arbitrary number of bins N_b of size δ is selected and the number of events k_i in each bin is quantified. The mean μ_k and variance σ_k^2 are calculated as follows

$$\mu_k = \frac{1}{N_b}\sum_{i=1}^{N_b} k_i \tag{8}$$

$$\sigma_k^2 = \frac{1}{N_b}\sum_{i=1}^{N_b} (\mu_k - k_i)^2 \tag{9}$$

The optimal bin size is the value of δ that minimizes the cost function $C(\delta)$

$$C(\delta) = \frac{2\mu_k - \sigma_k^2}{\delta^2} \tag{10}$$

For the histograms obtained in this investigation it was found that the Freedman-Diaconis and the Shimazaki and Shinomoto estimators yielded similar results with the optimal number varying from 185 to 204, respectively.

Numerical flow conditions

The 3-D modeling of the flow field requires the simultaneous numerical solution of the steady-state incompressible Navier-Stokes momentum (Eq. 11) and continuity (Eq. 12) tackled by means of the finite element method

$$\rho\left(\frac{\partial \mathbf{v}}{\partial t} + \mathbf{v}\cdot \text{grad } \mathbf{v}\right) = -\text{grad } p - \text{div } \tau \tag{11}$$

$$\text{div } \mathbf{v} = 0 \tag{12}$$

Where ρ is the fluid density, v is the velocity vector, p is the pressure, and ρ is the stress tensor. The 3-D solid models and the corresponding unstructured mesh were generated with GAMBIT (ANSYS, Inc.) software using block partitions to refine the mesh as required. Due to the complexity of the geometry and the aspect ratios of the microchannels, the final mesh required approximately 3.8 million elements for the SAR microreactor, and 6.1 million elements for the LLMR microreactor. The mesh of the LLMR required an increased number of elements due to the length of the 8 high-aspect ratio microchannels in the reaction section. To overcome this computationally expensive problem, the low-order MINI finite element[48] implemented in the commercial 3-D finite element software[49] POLY3D (Rheosoft, Inc.) was applied, yielding a total of approximately 2.2 million and 3.5 million equations for the SAR and LLMR, respectively. This type of finite element is inexpensive with respect to the number of degrees of freedom per element generated, which impact directly on the size of the final linear system. Due to the presence of the convective term in the Navier-Stokes equations, the problem is nonlinear. To solve the respective system of equations a Newton-Raphson iterative scheme was used. Convergence problems were encountered in preliminary simulations for the SAR microreactor due to the small volume size of the tetrahedral elements needed. The volume of the elements was calculated by dividing the active volume of the microreactor by the number of elements in the mesh yielding a volume of $\sim 4.3\cdot 10^{-14}$ m^3 per element. Since this value is close to the machine epsilon ($\sim 10^{-15}$), a change of units to millimeters and grams was mandatory to converge the solution of the flow solver.

The fluid properties considered for the simulations correspond to the flow of water in steady-state laminar regime. The flow conditions considered for the simulations are summarized in Table 2. The boundary conditions imposed are:

1 No-slip velocity at the wall surfaces;
2 Zero radial velocity at the inlets;
3 Parabolic velocity profile in the axial direction;
4 Free-flow condition in the axial direction at the outlet.

Particle tracking method

The particle tracking technique performed in this study is based on the methodology developed by Heniche and Tanguy.[50] Preliminary runs were performed on the SAR microreactor to determine the influence of the number of tracer particles injected. Five cases were investigated using 5,200, 13,000, 31,000, 63,000, and 100,000 tracer particles.

The injection consisted of a circular plane in which the tracer particles were evenly distributed covering only 94% of the radius of the inlet plane (3.175 mm and 1.59 mm for the SAR and LLMR, respectively). This value of 0.94R has been proposed by Nauman[51] as a guideline to avoid the injection of tracer particles in close proximity to the walls of the vessel, which would contribute to long tailing effects. Reference planes were defined at each inlet of the microchannels of the splitting manifolds as well as at the outlet plane of the mixing and reaction sections of the microreactors.

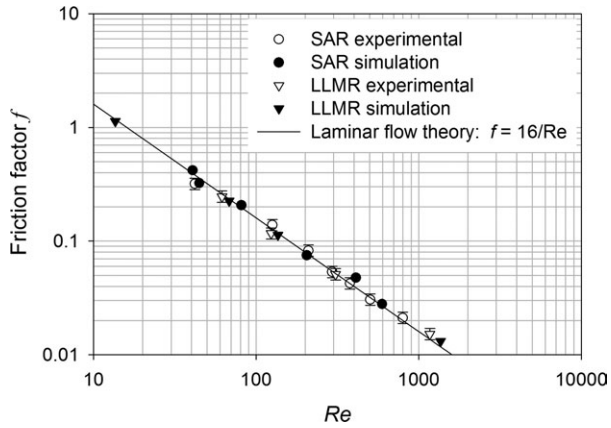

Figure 6. Comparison of the friction factor calculated from the numerical and experimental data for the SAR and LLMR microreactors.

The amount of tracer particles lost in each case was around 50–60%. It was found that neither the shape of the histogram nor the magnitudes of the first and second moment of the distributions were affected by the number of tracer particles injected. Thus, the rest of the analysis was performed using 5,200 tracer particles to reduce the computation time.

Results and Discussion

Pressure drop

The pressure drop values obtained from the simulations are compared to experimental data and converted to a nondimensional friction factor f. The conversion is made by calculating an equivalent dia. d_{eq}, that for a given flow rate would produce the same pressure drop as the microreactors. The numerical results are plotted in Figure 6 as a function of the Reynolds number calculated as

$$Re = \frac{\rho v d_{eq}}{\mu} \tag{13}$$

The numerical results show an excellent agreement with both laminar flow theory and experimental data. The numerical values for d_{eq} are 0.522 mm for the SAR and 0.311 mm for the LLMR, which are also in agreement with the respective values of 0.506 and 0.344 mm obtained from experiments. The flow rates of 0.2, 1.0, 2.0, and 20.0 mL/min correspond, respectively to Re values of 8, 41, 83 and 825 for the SAR, and 14, 68, 136 and 1363 for the LLMR.

Flow distribution

The flow rate delivered to each microchannel of the SAR has been normalized with the theoretical value expected in the situation of homogeneous distribution, i.e., 20% of the volumetric flow rate per inlet being delivered into each microchannel. It was found that for all the hydrodynamic conditions investigated there is an imbalance in the flow distribution in the SAR trapezoidal manifolds. Figure 7 shows the pathlines obtained in the manifold of inlet 1 at different flow conditions when $r_Q = 1$ (i.e., conditions 1, 4, 5 and 6). The pathlines have been normalized by the maximal flow velocity at each flow condition. The manifold of inlet 2 (not shown) exhibits the same trend.

The flow imbalance (Figure 8) exhibits an almost linear asymmetry with respect to the center channel with differences of approximately 5% per adjacent channel. The microchannel closest to its respective inlet receives as much as 10% more fluid than the center channel, while the microchannel farthest to the inlet exhibits a 10% deficit. However, a slight reduction in this difference is observed as the flow rate is increased. This suggests that a better flow distribution may be obtained at higher flow rates although at the expense of higher pressure drops.

The flow distribution in the LLMR (not shown) occurs after the mixing section and before entering the reaction passages. Although the distribution of flow does not have a direct impact on the mixing stage of the LLMR it was found that the axially symmetrical manifold design can produce a

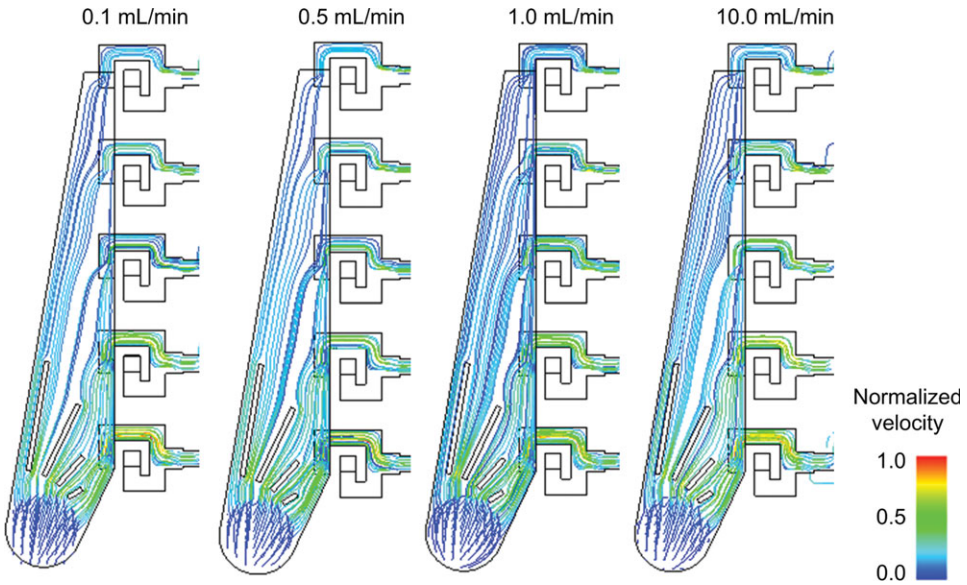

Figure 7. Fluid pathlines in the SAR manifold for different flow conditions when $r_Q = 1$.

[Color figure can be viewed in the online issue, which is available at wileyonlinelibrary.com.]

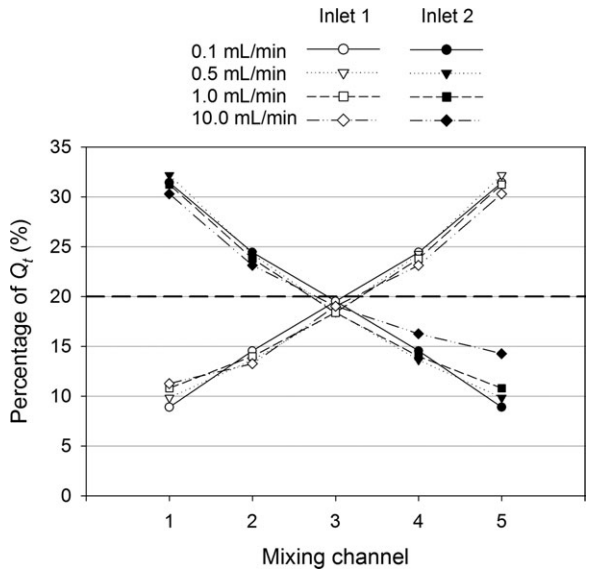

Figure 8. Percentage of the total flow rate that is delivered to each mixing microchannel in the SAR microreactor.

homogeneous flow distribution in parallel microchannel networks.

The flow imbalance is further verified using the particle tracking method. In an optimal flow distribution situation the total amount of particles detected at the entrance of each mixing microchannel of the SAR should be composed of an equal amount of particles coming from each inlet. For the three flow conditions with $r_Q = 1$ (Figure 9) the flow composition in each microchannel is nearly identical and follows the trend shown in Figure 8 where only the central channel achieves a 50/50 composition. There is approximately a 12.5% variation per adjacent channel with the ones closest to the inlets receiving as much as 25% more particles than the center channel.

For the case of different feeding ratios the volumetric flow rate of inlet 1 was kept constant at 0.1 mL/min while the flow rate of inlet 2 was increased from 0.1 mL/min to 1.0 and 10.0 mL/min. In this situation the effect of bypassing is observed with particles injected through inlet 1 flowing only through channels 4 and 5 when inlet 2 is at 1.0 mL/min and only through channel 5 when inlet 2 is increased to 10.0 mL/min. The tracer pathlines in Figure 10 (in red and blue) confirms a recirculation effect of the fluid delivered through inlet 2 (blue), and a bypassing effect of the fluid delivered through inlet 1 (red) when $r_Q \neq 1$. The recirculation of fluid delivered through inlet 2 around the G-shaped structures is produced by the pressure difference that forces the fluid into the distribution manifold of inlet 1. Upon colliding with the upcoming stream the fluid from inlet 1 is bypassed through a reduced number of channels.

At $r_Q = 0.01$, inlet 1 contributes as much as 85% of the total composition of the microchannel (Figure 11). The pressure imbalance has a great impact on the flow distribution capabilities of the trapezoidal manifold structure and renders the SAR microreactor as a less suitable alternative to be used, for instance, in emulsification processes since in such applications the droplet size and droplet-size distribution is frequently controlled by the ratio of flow rates.

Mixing characterization: Scale and intensity of segregation

The scale and intensity of segregation were evaluated at the outlet plane of the mixing section for both microreactors. The outlet planes of the mixing sections of the SAR and LLMR microreactors are circular and rectangular, respectively. A squared reference plane was used for the SAR, while a rectangular grid was used for the LLMR. To determine the influence of the grid size during the mixing analysis the scale and intensity of segregation of the SAR microreactor were calculated as a function of the total number of cells in the reference plane for two flow conditions with $r_Q = 1$. The maximum number of cells must not exceed the number of particles reaching the reference plane. The minimum number of tracer particles arrived at the reference plane was 4,935, thus, to avoid statistical distortion the maximum number of cells was fixed to 4,900 (i.e., 70 cells per side of a squared grid). The results in Figure 12 show that the magnitude of S_s does not follow a linear trend as a function of the cell number for the two flow conditions investigated. Interestingly, the difference between both conditions at each cell number remains constant regardless of the absolute value of S_s. The values of I_s show a linear increase as a function of the number of cells. This is due to the size of the individual grid cells in comparison to the scale of segregation of the tracer particles. If the cell size is lower than a limiting value of the scale of segregation, then the concentration of tracer particles in each cell will be likely to be either only A or B, thus, affecting the value of I_s. The limit of S_s is selected as the mean of the values in Figure 12. This mean of S_s at the exit of the mixing section of the microreactors was found to be 0.18 mm for the SAR and 0.03 mm for the LLMR.

The effect of the cell size on the value of I_s can be better observed in Figure 13, where the intensity of segregation of the SAR and LLMR for cell sizes lower and higher than the limit value of S_s are plotted as a function of the energy dissipation defined as

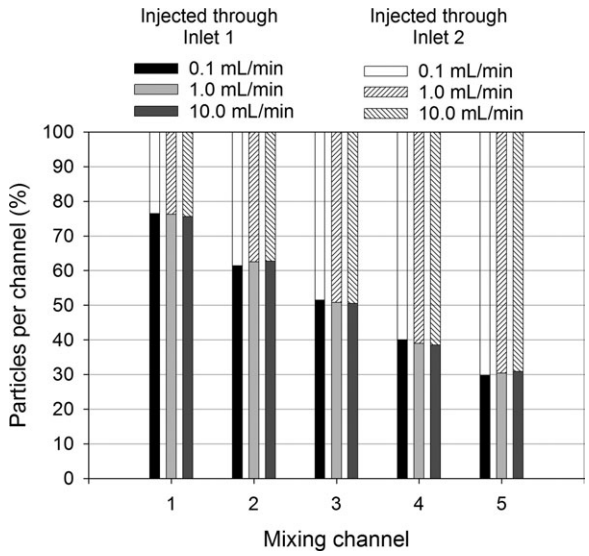

Figure 9. Percentage of particles injected through inlet 1 and inlet 2 that reach each mixing microchannel for $r_Q = 1$.

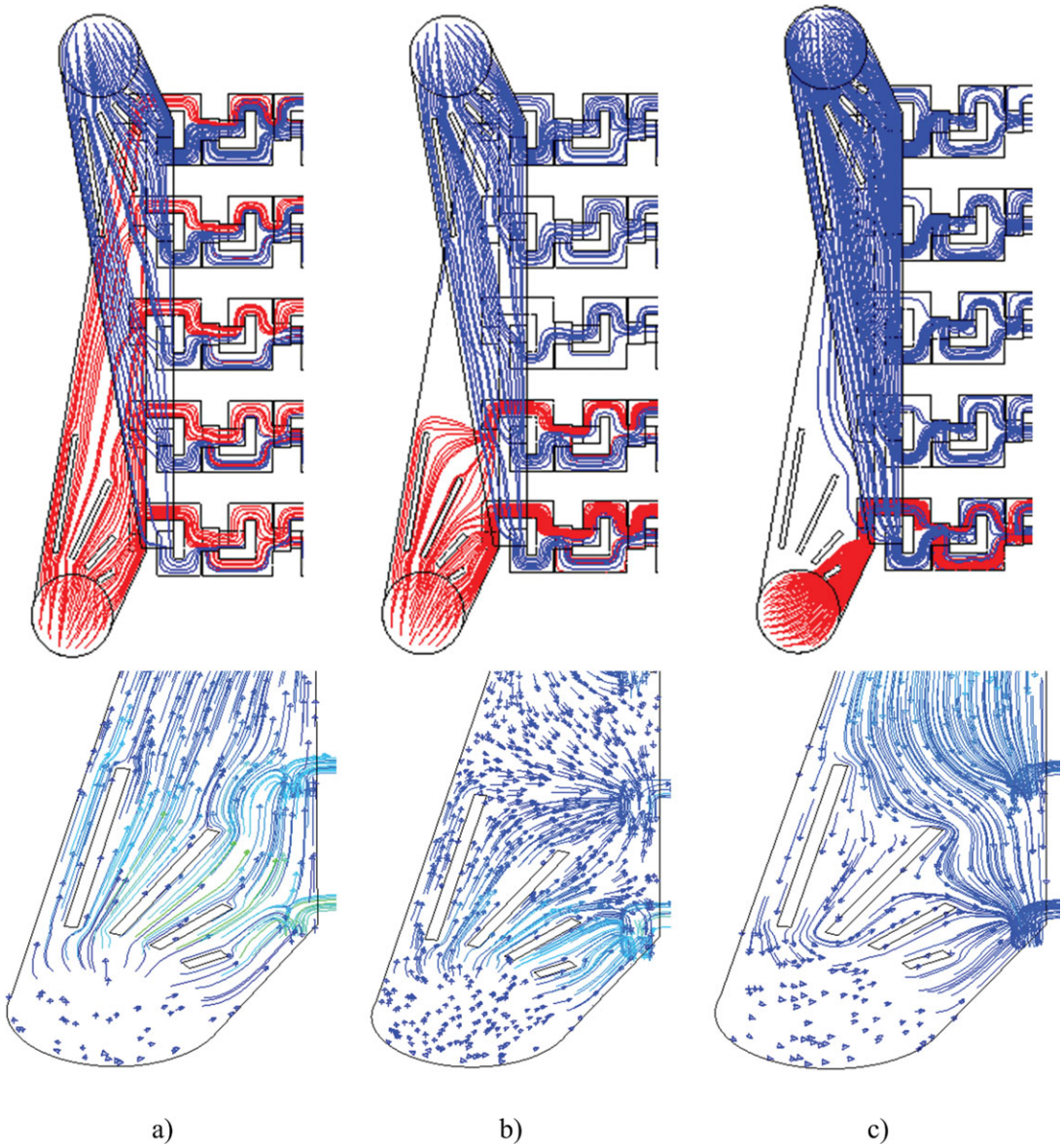

Figure 10. Details of the tracer pathlines in the manifolds of inlet 1 (red) and inlet 2 (blue) of the SAR microreactor (upper images); and velocity vectors in the manifold of inlet 1 (lower images) for different flow ratios (a) $r_Q = 1$, (b) $r_Q = 0.1$, and (c) $r_Q = 0.01$.

[Color figure can be viewed in the online issue, which is available at wileyonlinelibrary.com.]

$$\varepsilon = \frac{\Delta P \cdot v}{\rho \cdot l} \tag{14}$$

where v is the flow mean velocity, ρ is the mass density, and l is the microreactor or tube length between the pressure detection points. When the cell size is lower than the limit of S_s, the intensity of segregation is considerably increased.

Since the values of scale of segregation for the SAR and LLMR microreactors are in the range of ~0.1 mm and ~0.01 mm, respectively, then in the presence of molecular diffusion the LLMR will lead to shortest mixing times between fluid layers. One interesting result that deserves attention is that from a fluid mechanics perspective the intensity of segregation achieved by these microreactors is not significantly affected by the amount of energy applied to the system.

For the cases when the cell size is greater than the limiting value of S_s, the SAR mixing section achieves an average I_s value of 0.53. For the LLMR an average I_s value of 0.16 is reached except at 20.0 mL/min where a higher state of segregation (~0.58) is observed.

This behavior is analyzed in Figure 14 using Poincaré maps at the exit plane of the mixing section of the LLMR for different Re. In the context of CFD, a Poincaré map can be defined as the surface of intersection between the tracer particles and a subspace perpendicular to the fluid flow. It is worth to underline that the interdigital mixing structure of the LLMR produces an alternated pattern of layers of tracer particles. The ordered arrangement of the tracer particles is compressed in the center and stretched at the edges as the flow rate is increased. At $Re = 1363$ (20.0 mL/min) the layered and alternate arrangement is broken and while the value

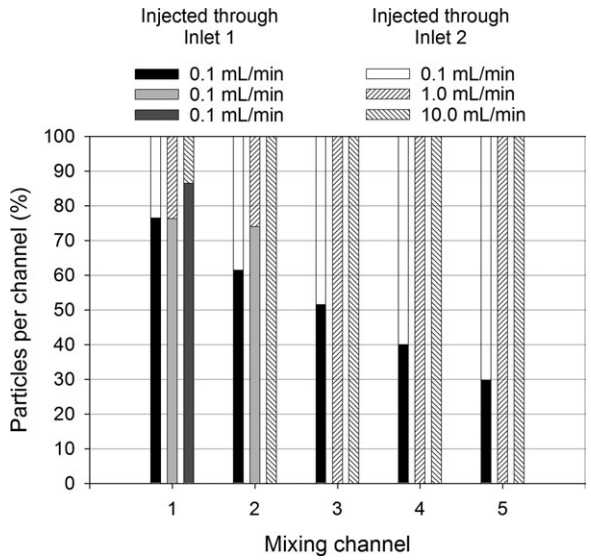

Figure 11. Percentage of particles injected through inlet 1 and inlet 2 that reach each mixing microchannel for $r_Q \neq 1$.

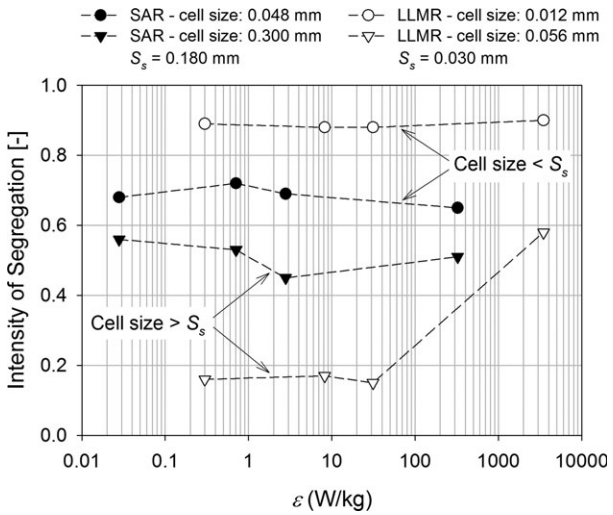

Figure 13. Intensity of segregation as a function of the power dissipation for the mixing section of the SAR and LLMR obtained using two different cell sizes.

of the scale of segregation remains close the mean value, the average value of I_s is increased from 0.16 to 0.58. The tracer particles at $Re = 1363$ are segregated in two major pockets along the longest dimension of the exit plane. The alternated arrangement produced by the LLMR geometry can be maintained for $Re < 140$.

The effect of r_Q on the values of I_s and S_s as well as on the disposition of the Poincaré maps for the LLMR is shown in Figure 15. As the flow ratio is decreased, a higher state of segregation is produced and a lower scale of segregation is achieved for the stream injected through inlet 1 (i.e., the fluid segments represented by the red particles); the opposite effect is observed for the stream supplied through inlet 2 (i.e., represented by the blue particles). Thus, for flow ratios different than one the intercalated arrangement generated by the interdigital structure is distorted and the layer thicknesses are disproportional as compared to the balanced condition when $r_Q = 1$.

The Poincaré maps at the exit of the mixing section of the SAR are shown in Figure 16. For $r_Q = 1$ (Figure 16a) the average values of S_s and I_s are 0.18 mm and 0.5, respectively. The cases for $r_Q \neq 1$ (Figure 16b) confirm the strong

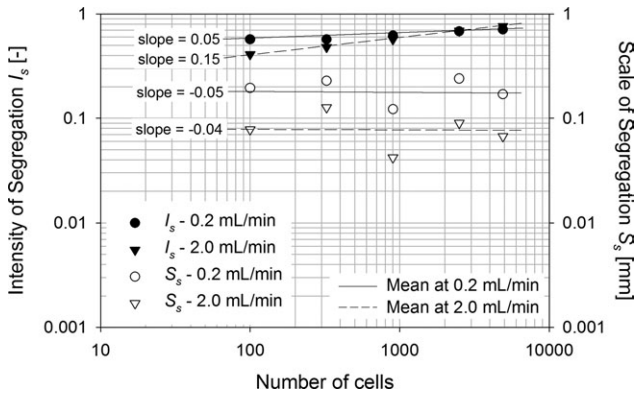

Figure 12. Scale and intensity of segregation of the SAR mixing section at two different flow conditions with $r_Q = 1$.

uneven distribution of tracer positions produced by the SAR manifolds. The scale of segregation diminishes for the red tracer particles (i.e., increases for the blue particles) as r_Q is increased. It can be seen that the Poincaré maps configuration depends on Re. More precisely, at low-velocity conditions the particles concentrate in one half section of the circular exit plane. Then, as Re increases the particles shift toward the center of the plane until arriving to the opposite half section. It was found that neither the number of tracer particles injected nor the grid size affect this behavior.

The control plane of the SAR microreactor is placed in the straight outlet tube as close as possible to the exit of the mixing section following a 90° bend, thus, the location of the tracer particles might be affected by inertial effects. For the SAR microreactor the corners of the grid outside the circular control plane were not included during the calculations, and the analysis of scale and intensity of segregation was conducted only in the zones were tracer particles were detected. The configuration of the Poincaré maps in Figure 16 strongly depends on Re and r_Q, thus, revealing the importance of the operating conditions on the mixing capabilities of the SAR microreactor. In our case we found that the condition at $Re = 83$ and $r_Q = 1$ yields the lowest value of scale and intensity of segregation.

Residence time distribution

The mean residence times (t_m) obtained numerically are listed in Table 3 along with the theoretical and experimental values previously obtained. In our previous experimental findings[28] it was found that the classical axial dispersion model (ADM) was capable of describing the microreactor behavior only at $Re = 6$ (0.2 mL/min) and that for $Re > 35$ a compartment flow model using a plug flow in series with the side capacity model provided a better fit. In the experimental scenario the molecular diffusion greatly contributed to the spread of the tracer at $Re = 6$. In this study, the particle tracking method disregards molecular diffusion, and, thus, the ADM was not capable to fit the SAR flow behavior. The microfluidic structure of the SAR microreactor can be regarded as a series of plug flow reactors with different

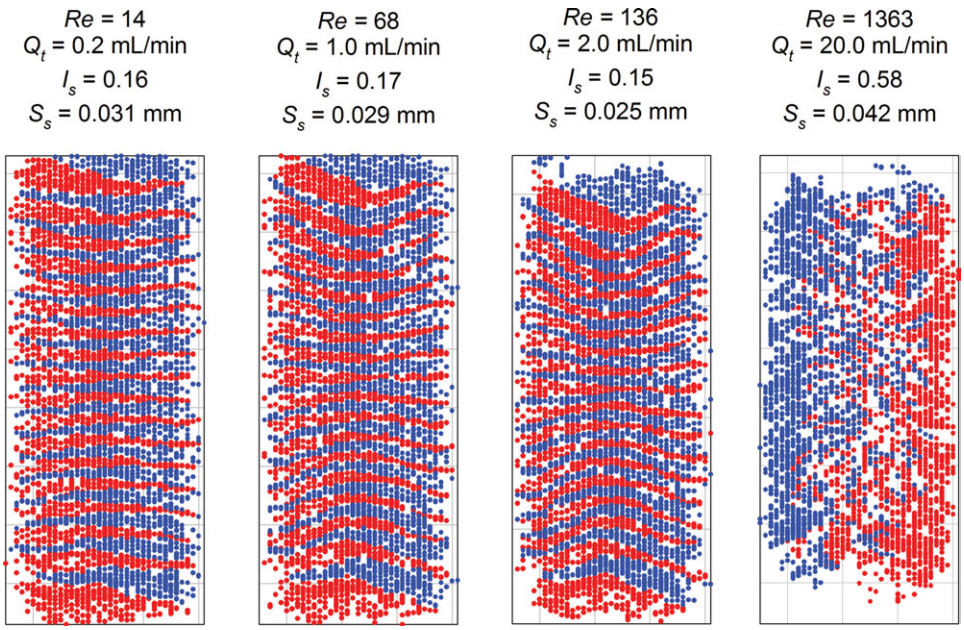

Figure 14. Poincaré maps produced by the interdigital structure of the LLMR for different *Re* with $r_Q = 1$.

[Color figure can be viewed in the online issue, which is available at wileyonlinelibrary.com.]

flow rates connected in parallel. Such flow arrangements are known to produce exponential decay curves rather than Gaussian distributions.[52] On the other hand, the mixing principle of the LLMR relies on the direct multilamination of flow by the interdigital structure and no recombination of fluid is performed during the mixing stage. Compared to the SAR, the LLMR resembles more closely the characteristics of an open pipe. Figure 17 shows the RTD curves of the mixing and reaction sections of both microreactors in dimensionless form.

In the absence of molecular diffusion the pure convection model[52] accurately describes the RTD of the microreactors under laminar flow regime. The convection model can be defined in dimensionless form as

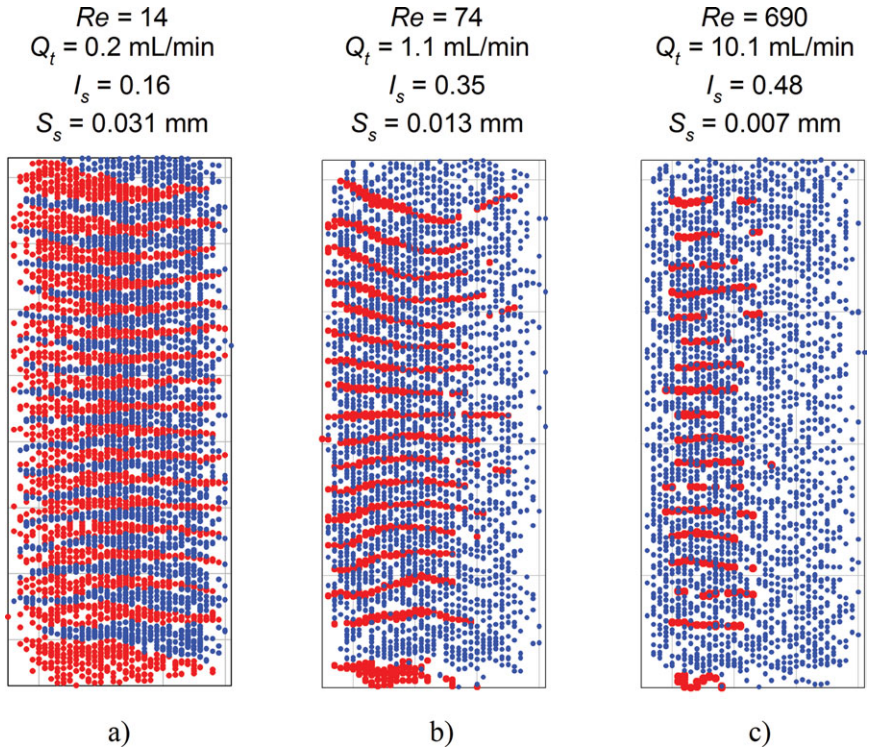

Figure 15. Poincaré maps generated by the interdigital structure of the LLMR for different flow ratios (a) $r_Q = 1$, (b) $r_Q = 0.1$, and (c) $r_Q = 0.01$.

[Color figure can be viewed in the online issue, which is available at wileyonlinelibrary.com.]

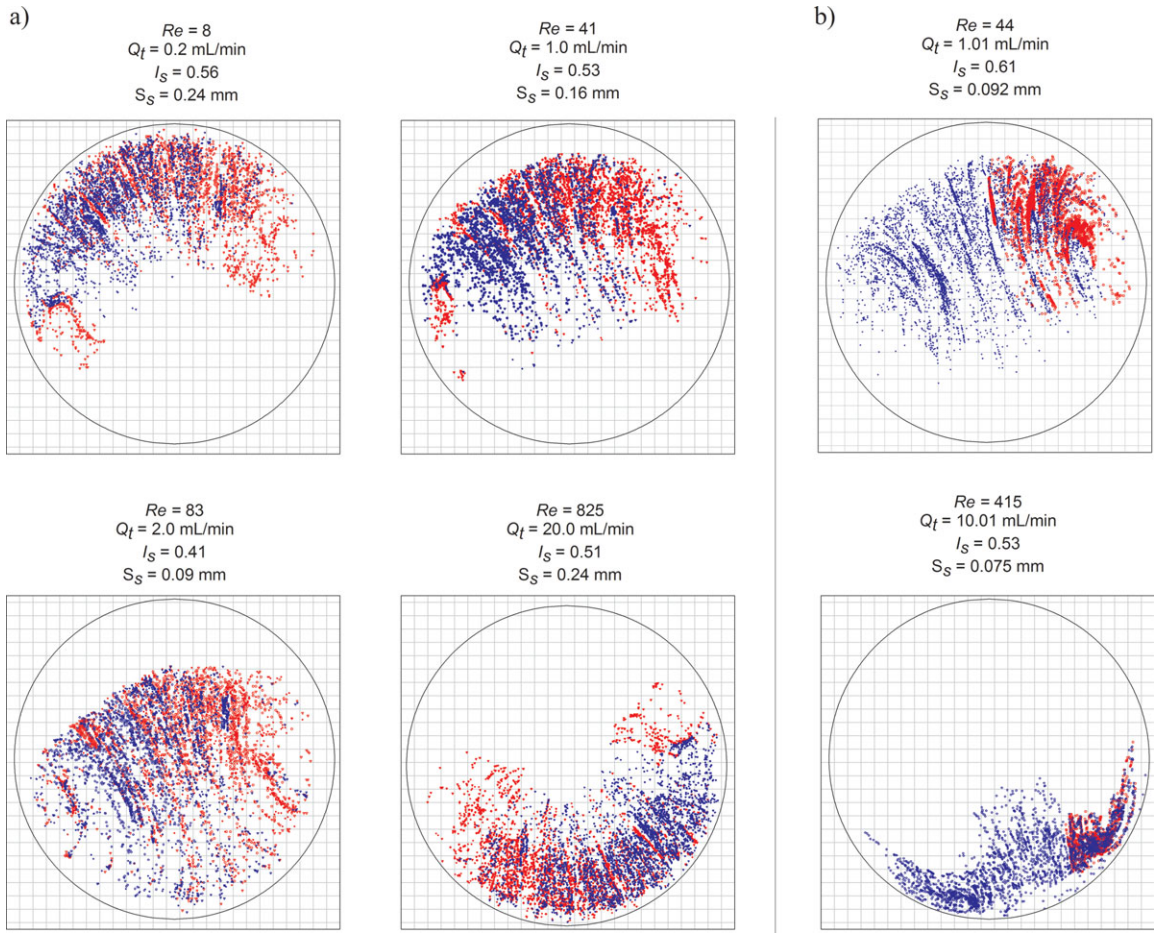

Figure 16. Poincare maps at the exit plane of the SAR mixing section at different *Re* (a) $r_Q = 1$, (b) $r_Q \neq 1$.

[Color figure can be viewed in the online issue, which is available at wileyonlinelibrary.com.]

$$E_\theta = \begin{cases} 0 & for \quad \theta < 0.5 \\ \frac{1}{2\theta^3} & for \quad \theta \geq 0.5 \end{cases} \tag{15}$$

where θ is defined as the time parameter t over the mean residence time t_m. Figure 17 provides no indication of recirculation or stagnancy when $r_Q = 1$. The reaction section of the LLMR is also well characterized by the pure convection model since the flow configuration comprises a set of parallel microchannels with equal volumetric rates of flow.

Conclusions

The pressure drop results of the SAR and LLMR microreactors are in excellent agreement with laminar flow theory and experimental results yielding tube-equivalent diameters of 0.522 mm and 0.311 mm, respectively.

It has been shown that with the SAR microreactor principle, the manifolds design produces an unbalanced flow distribution in the microchannel network. This imbalance results in variations of composition of 12.5% between adjacent microchannels. For the cases when an equal feeding ratio is used only the central microchannel achieves a 50/50 composition.

The visualization of the velocity fields by CFD and the mixing analysis with the particle tracking method confirm the presence of recirculation and bypassing in the SAR microfluidic structure for $r_Q \neq 1$. Thus, the use of feeding ratios other than one further deteriorates any flow imbalance already present due to the geometry of the distribution manifolds. Improved designs are required to make SAR microreactors industrially successful. While not directly affecting the mixing mechanism of the microreactor, the symmetrical manifold construction of the LLMR proved to evenly distribute the flow under all the conditions investigated and can be used as a guideline for the design optimization of microreactors requiring distribution of flow in several substreams.

The scale and intensity of segregation concepts originally proposed by Danckwerts allowed for the quantification of mixing efficiency by means of the particle tracking method. It was found that in the absence of molecular diffusion, the intensity and scale of segregation achieved by both microreactors at $r_Q = 1$ are not significantly affected by the

Table 3. Mean Residence Time of the SAR and LLMR Microreactors obtained by CFD

	Flow rate (mL/min)	Mean Residence Time t_m (s)			
		Experimental	Theory	CFD	Error (%)
SAR	0.2	79.73 ± 1.18	57.27	57.58	0.6
	1.0	11.25 ± 0.85	11.45	10.91	4.8
	2.0	5.84 ± 0.19	5.72	5.51	3.8
	20.0	0.57 ± 0.01	0.57	0.58	2.8
LLMR	0.2	38.53 ± 3.45	39.91	36.67	8.1
	1.0	6.18 ± 0.19	7.98	7.40	7.2
	2.0	3.79 ± 0.23	3.98	3.75	5.9
	20.0	0.37 ± 0.02	0.39	0.35	10.1

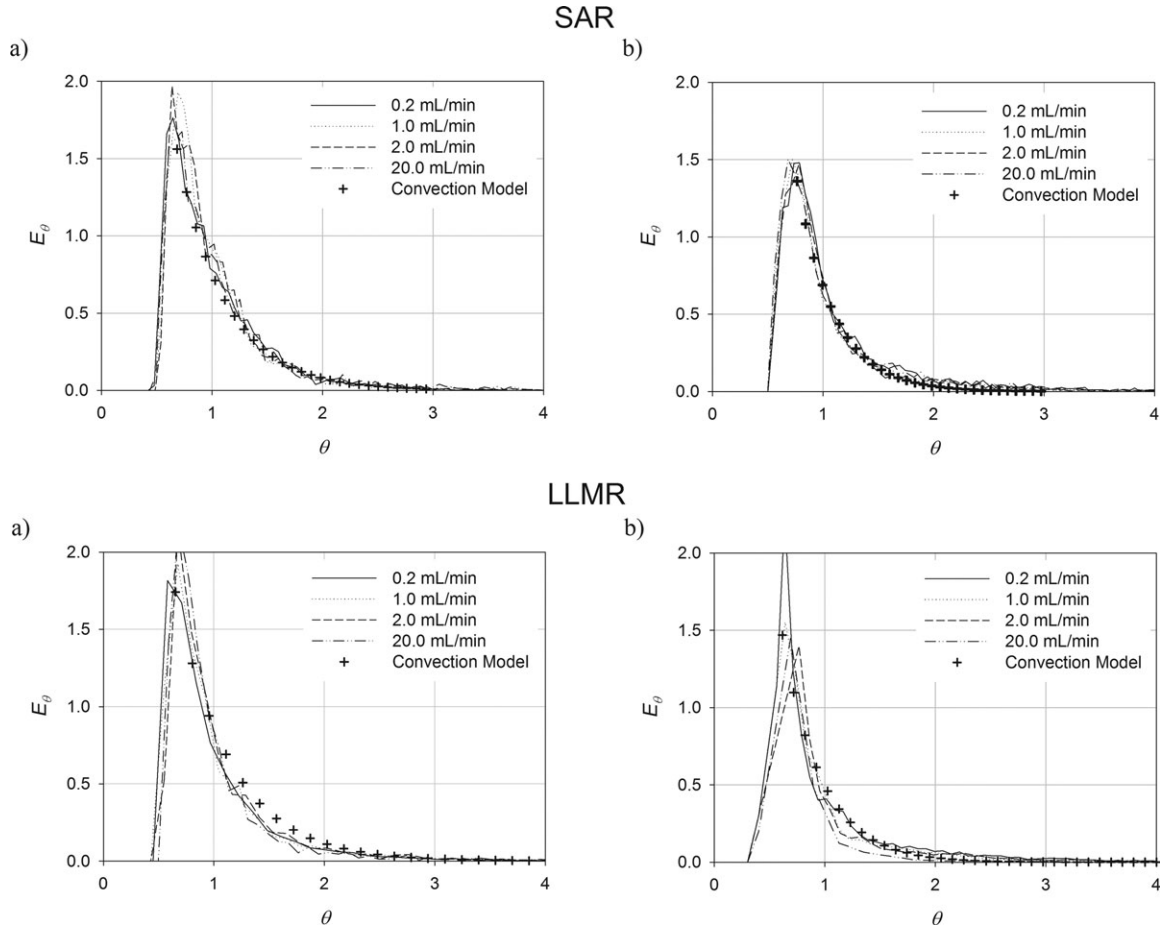

Figure 17. RTD functions in dimensionless form obtained numerically for the SAR and LLMR microreactors (a) mixing section, and (b) reaction section.

amount of energy applied to the system except for the LLMR at $Re = 1363$. In contrast, these same characteristics were considerably affected at $r_Q \neq 1$ proving that unbalanced flow ratios are not the optimal operating conditions for the mixing mechanisms of both microreactors. The RTD obtained by means of CFD were accurately described by the pure convection flow model and the shape of the curves showed that the mixing and reaction sections of both microreactors exhibit the behavior of tubular reactors under laminar flow conditions with no recirculation or stagnancy present for $r_Q = 1$.

Acknowledgments

The authors thank Atotech GmbH (Berlin, Germany) for providing the SAR microreactor. Also, we gratefully acknowledge the financial support from the Natural Science and Engineering Research Council of Canada (NSERC), the National Council of Science and Technology of Mexico (CONACYT) and the oil company TOTAL.

Notation

a = concentration of species a in terms of volume fraction, dimensionless
A_{in} = total area of inlet plane, m^2
b = concentration of species b in terms of volume fraction, dimensionless
C = cost function, dimensionless
COV = coefficient of variance, dimensionless
I_s = intensity of segregation, dimensionless
J = content of particles in a line-sample, particles·mm
k_i = number of counts per bin
N_b = total number of bins
N_t = total number of tracer particles
Q = volumetric flow rate, m^3/s
r = radial position of the tracer particles, m
r_Q = ratio of flow rates
R = radius of the inlet tube, m
s = standard deviation
S_s = scale of segregation, mm
t = time, s
t_m = mean residence time, s
v = mean velocity, m/s
v = velocity vector, m/s
V = volume, m^3
X = Line-sample, mm
δ = size of histogram bin
μ_k = mean value of counts per bin
ρ = mass density, kg/m^3
σ^2 = variance of quantity denoted by subscript
τ = stress tensor, Pa
θ = dimensionless time parameter

Literature Cited

1. Bayer T, Pysall D, Wachsen O. Micromixing effect in continuous radical polymerization. Microreaction Technology: 3rd International Conference on Microreaction Technology, Proceedings of IMRET 3, Springer-Verlag, Berlin; 2000:165–170.
2. Wörz O, Jäckel KP, Richter T, Wolf A. Microreactors - A new efficient tool for reactor development. *Chem Eng Tech.* 2001;24(2):138–142.
3. Yoshida J, Nagaki A, Iwasaki T, Suga S. Enhancement of chemical selectivity by microreactors. *Chem Eng Tech.* 2005;28(3):259–266.

4. Mengeaud V, Josserand J, Girault HH. Mixing processes in a zigzag microchannel: Finite element simulations and optical study. *Anal Chem*. 2002;74(16):4279–4286.
5. Stroock AD, Dertinger SK, Whitesides GM, Ajdari A. Patterning flows using grooved surfaces. *Anal Chem*. 2002;74(20):5306–5312.
6. Stroock AD, Dertinger SKW, Ajdari A, Mezic I, Stone HA, Whitesides GM. Chaotic mixer for microchannels. *Science*. 2002;295(5555):647–651.
7. Hardt S, Schonfeld F. Laminar mixing in different interdigital micromixers: II. Numerical simulations. *AIChE J*. 2003;49(3):578–584.
8. Kim SJ, Kim D, Lee DY. On the local thermal equilibrium in microchannel heat sinks. *Int J Heat Mass Trans*. 2000;43(10):1735–1748.
9. Gobby D, Angeli P, Gavriilidis A. Mixing chacteristics of T-type microfluidic mixers. *J Micromech Microeng*. 2001;11(2):126–132.
10. Chen Y, Cheng P. Heat transfer and pressure drop in fractal tree-like microchannel nets. *Int J Heat Mass Trans*. 2002;45(13):2643–2648.
11. Commenge JM, Falk L, Corriou JP, Matlosz M. Optimal design for flow uniformity in microchannel reactors. *AIChE J*. 2002;48(2):345–358.
12. Tonomura O, Tanaka S, Noda M, Kano M, Hasebe S, Hasimoto I. CFD-based optimal design of manifold in plate-fin microdevices. *Chem Eng J*. 2004;101(1–3):397–402.
13. Aubin J, Fletcher DF, Bertrand J, Xuereb C. Characterization of the mixing quality in micromixers. *Chem Eng Tech*. 2003;26(12):1262–1270.
14. Engler M, Kockmann N, Kiefer T, Woias P. Numerical and experimental investigations on liquid mixing in static micromixers. *Chem Eng J*. 2004;101(1–3):315–322.
15. Wong SH, Ward MCL, Wharton CW. Micro T-mixer as a rapid mixing micromixer. *Sens Actuators B Chem*. 2004;100(3):359–379.
16. Aubin J, Fletcher DF, Xuereb C. Design of micromixers using CFD modelling. *Chem Eng Sci*. 2005;60(8–9):2503–2516.
17. Serra C, Sary N, Schlatter G, Hadziioannou G, Hessel V. Numerical simulation of polymerization in interdigital multilamination micromixers. *Lab Chip*. 2005;5(9):966–973.
18. Kockmann N, Kiefer T, Engler M, Woias P. Convective mixing and chemical reactions in microchannels with high flow rates. *Sens Actuators B Chem*. 2006;117(2):495–508.
19. Gamrat G, Favre-Marinet M, Le Person S, Baviere R, Ayela F. An experimental study and modelling of roughness effects on laminar flow in microchannels. *J Fluid Mech*. 2008;594:399–423.
20. Lee SW, Lee SS. Rotation effect in split and recombination micromixing. *Sens Actuators B Chem*. 2008;129(1):364–371.
21. Yu L, Nassar R, Fang J, Kuila D, Varahramyan K. Investigation of a novel microreactor for enhancing mixing and conversion. *Chem Eng Comm*. 2008;195(7):745–757.
22. Cortes-Quiroz CA, Azarbadegan A, Zangeneh M, Goto A. Analysis and multi-criteria design optimization of geometric characteristics of grooved micromixer. *Chem Eng J*. 2010;160(3):852–864.
23. Adeosun JT, Lawal A. Mass transfer enhancement in microchannel reactors by reorientation of fluid interfaces and stretching. *Sens Actuators B Chem*. 2005;110(1):101–111.
24. Adeosun JT, Lawal A. Numerical and experimental studies of mixing characteristics in a T-nuction microchannel using residence-time distribution. *Chem Eng Sci*. 2009;64:2422–2432.
25. Aubin J, Prat L, Xuereb C, Gourdon C. Effect of microchannel aspect ratio on residence time distributions and the axial dispersion coefficient. *Chem Eng Process*. 2009;48(1):554–559.
26. Cantu-Perez A, Bi S, Barrass S, Wood M, Gavriilidis A. Residence time distribution studies in microstructured plate reactors. *J Appl Thermal Eng*. 2010;In Press. doi:10.1016/j.applthermaleng.2010.04.024.
27. Cantu-Perez A, Barrass S, Gavriilidis A. Residence time distributions in microchannels: Comparison between channels with herringbone structures and a rectangular channel. *Chem Eng J*. 2010;160(3):834–844.
28. Méndez-Portillo LS, Fradette L, Dubois C, Tanguy PA. Characterization of the Hydrodynamics and Mixing Performance of a split-and-recombination (SAR) prototype microreactor and a multilamination commercial microreactor. *Ind Eng Chem Res*. 2011. doi: 10.1021/ie102410b.
29. Antes J, Boskovic D, Krause H et al. Analysis and improvement of strong exothermic nitrations in microreactors. *Chem Eng Res Des*. 2003;81(7):760–765.
30. Ferstl W, Loebbecke S, Antes J et al. Development of an automated microreaction system with integrated sensorics for process screening and production. *Chem Eng J*. 2004;101(1–3):431–438.
31. Boskovic D, Loebbecke S. Modelling of the residence time distribution in micromixers. *Chem Eng J*. 2008;135(suppliment 1):S138–S146.
32. Hessel V, Hardt S, Löwe H. *Chemical Micro Process Engineering: Fundamentals, Modelling and Reactions*. Weinheim: Wiley-VCH; 2004.
33. Cerbelli S, Adrover A, Creta F, Giona M. Foundations of laminar chaotic mixing and spectral theory of linear operators. *Chem Eng Sci*. 2006;61(9):2754–2761.
34. Heniche M, Tanguy PA, Reeder MF, Fasano JB. Numerical investigation of blade shape in static mixing. *AIChE J*. 2005;51(1):44–58.
35. Rauline D, Tanguy PA, Le Blevec JM, Bousquet J. Numerical investigation of the performance of several static mixers. *Can J Chem Eng*. 1996;76:527–535.
36. Rauline D, Le Blevec JM, Bousquet J, Tanguy PA. A comparative assessment of the performance of the Kenics and SMX static mixers. *Chem Eng Res Des*. 2000;78(3):389–396.
37. Danckwerts PV. The definition and measurements of some characteristic mixtures. *Appl Sci Res*. 1952;A3:279.
38. Bandarapu B. Evaluation of Highly Viscous Liquid Mixing Based on Particle Tracking [PhD Thesis]: Dept of Chemistry, University of Paderborn; 2008.
39. Tanguy PA, Fradette L, Heniche M, Jaffer SA. *CFD Simulations of Static Mixers: A Survey*. In: Manas-Zloczower I, ed. *Mixing and Compounding of Polymers - Theory and Practice*. Cincinnati, OH: Hanser; 2009:304–307.
40. Rosander AC. *Elementary Principles of Statistics*. Toronto, Canada: D. Van Nostrand Co., Inc.; 1957.
41. Nauman EB. Residence time theory. *Ind Eng Chem Res*. 2008;47:3752–3766.
42. Hobbs DM, Muzzio FJ. The Kenics static mixer: a three-dimensional chaotic flow. *Chem Eng J*. 1997;67(3):153–166.
43. Wörner M. Approximate residence time distribution of fully develop laminar flow in a straight rectangular channel. *Chem Eng Sci*. 2010;65(11):3499–3507.
44. Nauman EB. The residence time distribution for laminar flow in helically coiled tubes. *Chem Eng Sci*. 1977;32:287–293.
45. Nauman EB. On residence time and trajectory calculations in motionless mixers. *Chem Eng J*. 1991;47:141–148.
46. Freedman D, Diaconis P. On the histogram as a density estimator: L_2 Theory. *Probab Theory Related Fields*. 1981;57(4):453–476.
47. Shimazaki H, Shinomoto S. A method for selecting the bin size of a time histogram. *Neural Comput*. 2007;19(6):1503–1527.
48. Arnold D, Brezzi F, Fortin M. A stable finite element for the stokes equations. *Calcolo*. 1984;21(4):337–344.
49. Coesnon B, Heniche M, Devals C, Bertrand F, Tanguy PA. A fast and robust fictitious domain method for modelling viscous flows in complex mixers: The example of propellant make-down. *Int J Numer Meth Fluids*. 2008;58(4):427–449.
50. Heniche M, Tanguy PA. A new element-by-element method for trajectory calculations with tetrahedral finite element meshes. *Int J Numer Meth Eng*. 2006;67(9):1290–1317.
51. Nauman EB. *Chemical Reactor Design, Optimization and Scaleup*. 2nd ed. Hoboken, NJ: John Wiley & Sons, Inc.; 2008.
52. Levenspiel O. *Chemical Reaction Engineering*. New York, NY: John Wiley &Sons, Inc.; 1999.

Manuscript received Feb. 9, 2011, and revision received Jan. 13, 2012, and final revision received May 23, 2012.